

A Simple Route to Synthesize Mesoporous ZSM-5 Templated by Ammonium-Modified Chitosan**

Junjiang Jin,^[a] Xingdi Zhang,^[a] Yongsheng Li,^{*,[a]} Hua Li,^[a] Wei Wu,^[b] Yunlong Cui,^[a] Qian Chen,^[a] Liang Li,^[a] Jinlou Gu,^[a] Wenru Zhao,^[a] and Jianlin Shi^{*,[b]}

Abstract: Uniform mesoporous zeolite ZSM-5 crystals have been successfully fabricated through a simple hydrothermal synthetic method by utilizing ammonium-modified chitosan and tetrapropylammonium hydroxide (TPAOH) as the meso- and microscale template, respectively. It was revealed that mesopores with diameters of 5–20 nm coexisted with microporous network within

mesoporous ZSM-5 crystals. Ammonium-modified chitosan was demonstrated to serve as a mesoporegen, self-assembling with the zeolite precursor through strong static interactions. As

Keywords: ammonium • chitosan • heterogeneous catalysis • self-assembly • zeolites

expected, the prepared mesoporous ZSM-5 exhibited greatly enhanced catalytic activities compared with conventional ZSM-5 and Al-MCM-41 in reactions involving bulky molecules, such as the Claisen–Schmidt condensation of 2-hydroxyacetophenone with benzaldehyde and the esterification reaction of dodecanoic acid and 2-ethylhexanol.

Introduction

In the past decade, hierarchically porous materials with well-defined pore dimensions and architectures have gained increasing attention due to the multiple benefits from the combination of different pore-size systems within one unit.^[1] For instance, the presence of macro- and mesoporosity can improve the mass transport, which is very important in the processes involving bulky molecules, whereas the presence of meso- and microporosity would provide a large surface area for the high dispersion of active sites.^[1a,b,d] Mesoporous zeolites are one typical example of such hierarchical materials.

Crystalline zeolites are among the most important catalysts in industry, which have been widely used in oil refining, organic synthesis, and environmental fields due to their large specific surface area, high adsorption capacity, uniform

and intricate channels, high thermal and hydrothermal stabilities, and well-defined micropores with excellent shape-selectivity in catalysis.^[2] However, zeolite catalysts often suffer from the slow diffusion of reactants and products in their relatively small pore channels (<1.5 nm),^[2a,b,3] especially for bulky molecules. To overcome this drawback, various attempts have been made, such as the synthesis of zeolite nanocrystals,^[4] ultra-large pore zeolites,^[2a,b,5] supported zeolite crystals,^[6] and ordered mesoporous materials.^[7]

Zeolite nanocrystals expose more active sites than conventional zeolite crystals due to their larger external surface area. However, the difficulty to separate zeolite nanocrystals from the slurry mixture remains a problem in liquid-phase reactions.^[3a] The successful synthesis of ultra-large pore zeolites provides one route to solve the limitation of mass transfer and catalytic conversion in which bulky molecules are involved, but the high cost of employing specific organic templates and the relatively low stability hinder their wide applications in industry.^[8] The challenge of supported zeolite crystals is the demand of hydrothermally stable and alkali-tolerable porous supports. In the past two decades, the successful synthesis of ordered mesoporous materials opens a new avenue to overcome this drawback of microporous zeolites. Unfortunately, it is the amorphous nature of the mesoporous wall that determines their low hydrothermal stability and acidity compared with zeolite crystals.^[2a,b] Therefore, it is highly desirable to enhance the hydrothermal stability and acidity of mesoporous aluminosilicates. Mesoporous zeolites, which combine the advantages of microporous materials with high activity and stability and of mesoporous materials with large mesoporosity, are the most promising materials.

A wide variety of strategies have been developed to introduce mesoporosity into zeolite crystals, such as the post-treatment of zeolites by steaming, acid or base leaching,^[9]

[a] Dr. J. Jin, X. Zhang, Prof. Y. Li, Dr. H. Li, Y. Cui, Q. Chen, Dr. L. Li, Dr. J. Gu, Dr. W. Zhao
Key Laboratory for Ultrafine Materials
of Ministry of Education
School of Materials Science and Engineering
East China University of Science and Technology
No. 130 Mei-long Road, Shanghai 200237 (P.R. China)
Fax: (+86)21-64250740
E-mail: ysli@ecust.edu.cn

[b] W. Wu, Prof. J. Shi
State Key Laboratory of
High Performance Ceramics and Superfine Microstructures
Shanghai Institute of Ceramics, Chinese Academy of Science
No. 1295 Ding-xi Road, Shanghai 200050 (P.R. China)
E-mail: jlshi@mail.sic.ac.cn

[**] ZSM = Zeolite socony mobil.

Supporting information for this article is available on the WWW under <http://dx.doi.org/10.1002/chem.201201614>.

the assembly of zeolite nanocrystals without any secondary porogen,^[10] and the creation of mesopores by using nanostructured carbons,^[11] polymers,^[12] surfactants^[13] and inorganic nanoparticles.^[14] Recently, Ryoo and co-workers fabricated truly ordered mesoporous mordenite framework inverted (MFI) by using linear gemini-type templates consisting of several bridged ammonium cations terminated by long alkyl chains.^[13j] To avoid the phase-separation process between the mesopore and the crystalline wall, a number of attempts have been made, including using cationic polymer or surfactant template,^[12c,f,13a,b,k] silane-functionalized surfactant or polymer,^[12b,13c] steam-assisted crystallization,^[11a,f,12g,13j] and dense mesopore/silica composite hydrothermal crystallization.^[11b,c,12d] However, the above syntheses employed the elaborately built “hard” porogens including carbon nanotubes, carbon particles and pre-organized carbon scaffolds, or soft templates, such as specially designed dual-functional and environmental-unfriendly surfactants, which involved either multi-step procedures or less cost-effective templates in the synthesis. Therefore, the simple synthesis of mesoporous zeolites by using more conventional, environmentally friendly and cost-effective templates is still a challenge.

Chitosan, or poly(β -(1-4)-2-amino-2-deoxy-D-glucose), is the deacetylated natural product of chitin by simple alkali treatment, which is an abundant, low-cost, highly environmentally friendly and biocompatible biopolymer in the exoskeleton of crustaceans. The porogenic capability of chitosan was verified in literature by using titania or silica as the inorganic component in the composites.^[15] Recently, amorphous mesoporous silica–alumina was synthesized by means of the formation of inorganic–organic composites with the addition of chitosan biopolymer, and enhanced activity and accessibility were observed in the chitosan-containing catalyst.^[16] Unfortunately, however, its indissolubility under basic condition, which is usually required in the crystallization of zeolites, makes it difficult to synthesize mesoporous zeolites using chitosan biopolymer as mesoporegens. To the best of our knowledge, there are no reports on the synthesis of mesoporous zeolites using chitosan as mesoporegens directly to date.

The success of using cationic polymers in such a synthesis inspired us to functionalize the chitosan with ammonium for improving its base-dissolubility and enhancing the interaction between positively charged ammonium-modified chitosan and the negatively charged inorganic precursor simultaneously. Moreover, the higher thermal stability of ammonium-modified chitosan assures its high dispersion in the zeolite synthesis systems without decomposition.^[17]

In this work, we first synthesized cationic *N*-(2-hydroxy)propyl-3-trimethylammonium chitosan chloride (HTCC) by the reaction of glycidyltrimethylammonium chloride (GTMAC) and chitosan, and investigated its potentiality as the meso-template in the hydrothermal synthesis of mesoporous ZSM-5 material. Various technologies including XRD, N₂ adsorption, SEM, TEM, NMR spectroscopy, TGA, and temperature-programmed desorption (NH₃-TPD) were em-

ployed to characterize the obtained products. Its catalytic activity was verified in reactions involving bulky molecules, the Claisen–Schmidt condensation of 2-hydroxyacetophenone with benzaldehyde and the esterification reaction of lauric acid with 2-ethylhexanol, compared with those of conventional ZSM-5 and Al-MCM-41.

Results and Discussion

Ammonium-modified chitosan, *N*-(2-hydroxy)propyl-3-trimethylammonium chitosan chloride (HTCC) was obtained by the reaction of glycidyltrimethylammonium chloride (GTMAC) and chitosan. The FTIR spectra of chitosan and HTCC are presented in Figure S1 in the Supporting Information. In spectrum a, the broad peak at 3400–3000 cm⁻¹, as well known, can be attributed to O–H and N–H stretching vibrations, and the peak at 1600 cm⁻¹ corresponds to NH₂ deformation. In the spectrum b, a new peak positioned at 1485 cm⁻¹ appears, which corresponds to the C–H bending of methyl groups of quaternary ammonium, indicating the introduction of quaternary ammonium group on the HTCC chains. Moreover, compared with the negligible change in the characteristic peaks of primary alcohol and secondary alcohol between 1110 and 1070 cm⁻¹, the peak at 3400–3000 cm⁻¹ becomes sharper and the peak at 1600 cm⁻¹ disappears in the spectrum b, demonstrating that GTMAC mainly reacted with NH₂ groups in chitosan rather than with the OH groups.^[17] Due to the introduction of cationic ammonium groups into the chitosan chains, the dissolubility of HTCC is greatly improved, as shown in Figure S2 in the Supporting Information, whose solution is transparent without any precipitate.

Figure 1a shows the XRD patterns of mesoporous ZSM-5 (designated as MZ) and conventional ZSM-5. MZ exhibits the characteristic peaks associated with the MFI zeolite structure, the same as that of conventional ZSM-5. The comparable intensity shows that the addition of HTCC did not affect the crystallization significantly.

N₂ adsorption-desorption isotherms and Barrett–Joyner–Halenda (BJH) pore-size distribution of MZ and conventional ZSM-5 are given in Figure 1b. Conventional ZSM-5 exhibits a representative type I (Langmuir) isotherm according to the classification of IUPAC, which is characteristic of microporous materials. In contrast, the isotherm of MZ presents a notably mixture of type I and IV, with a larger adsorption amount and a broad hysteresis loop at the relative pressure of 0.6–0.9, indicating the presence of mesoporosity in MZ crystals. Accordingly, the BJH pore-size distribution of MZ derived from the desorption branch reveals the presence of mesopores in sample MZ of 5–20 nm in diameter (Figure 1b, inset), again confirming the presence of mesoporosity. As summarized in Table 1, the specific surface area (422 m² g⁻¹), external specific surface area (238 m² g⁻¹), total pore volume (0.42 cm³ g⁻¹), and external volume (0.34 cm³ g⁻¹) of MZ are larger than those of conventional ZSM-5 due to the introduction of mesoporosity. Such in-

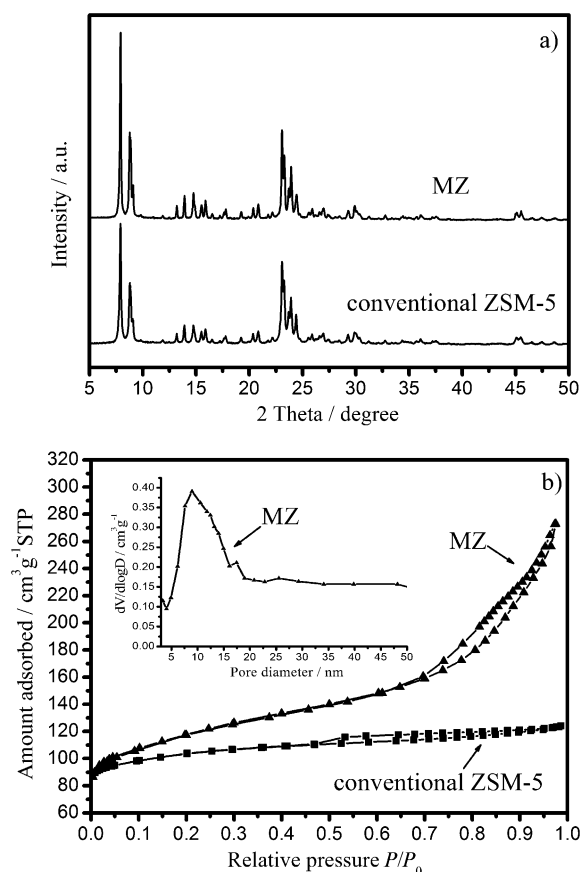


Figure 1. a) XRD pattern and b) N_2 sorption isotherms and pore-size distribution curve (inset in b) of conventional ZSM-5 and MZ.

creases are believed to facilitate catalytic reactions involving bulky molecules, despite a slight decrease in the zeolite crystallinity.^[12c]

Scanning electron microscopy (SEM) and transmission electron microscopy (TEM) observations provide detailed insights into the morphology and structure of the samples. Figure 2a and b clearly show that MZ particles exhibit extremely rough surfaces and are composed of uniform and fluffy cylindrical-like particles, about 250×500 nm in size. Mesopores estimated to be 5–20 nm within particles can be clearly observed in Figure 2b, open at the external surface

Table 1. Textural properties of the samples.^[a]

Sample	S_{BET} [$\text{m}^2 \text{g}^{-1}$]	S_{micro} [$\text{m}^2 \text{g}^{-1}$]	S_{external} [$\text{m}^2 \text{g}^{-1}$]	V_{total} [$\text{cm}^3 \text{g}^{-1}$]	V_{micro} [$\text{cm}^3 \text{g}^{-1}$]	V_{external} [$\text{cm}^3 \text{g}^{-1}$]	Mesopore diameter [nm]
MZ	422	184	238	0.42	0.08	0.34	5–20
Conventional ZSM-5	395	287	108	0.19	0.11	0.08	–
Al-MCM-41	966	–	966	0.87	–	0.87	2.7

[a] BET surface area (S_{BET}) is calculated from Brunauer–Emmett–Teller method; the micropore surface area (S_{micro}), external specific surface area (S_{external}) and the micropore volume (V_{micro}) are calculated from t-plot method; the total pore volume (V_{total}) is evaluated at $P/P_0=0.98$; the external pore volume (V_{external}) is calculated according to $V_{\text{total}}-V_{\text{micro}}$; the diameter of mesopore is estimated from BJH method using the desorption branch of the isotherm curves.

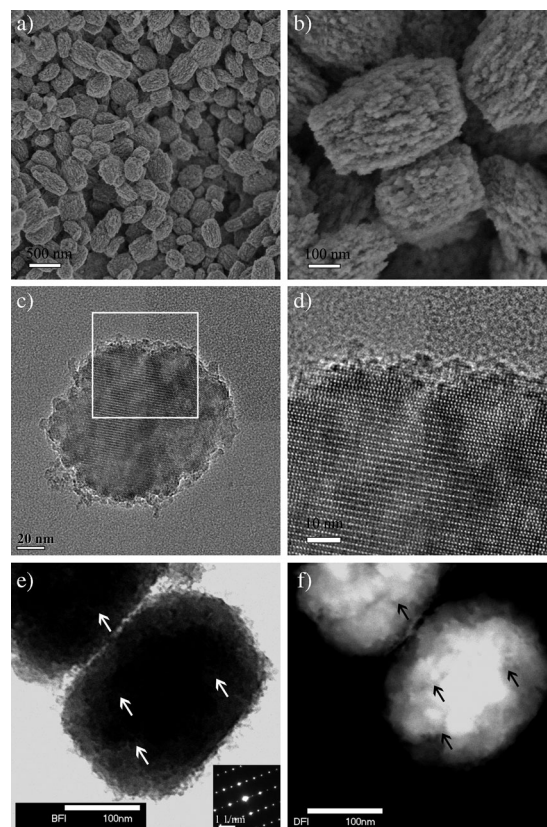


Figure 2. a) and b) SEM images of MZ under different magnifications; c) HR-TEM image of MZ; d) HR-TEM image from the area marked by a white square in c); e) bright-field image of MZ and its corresponding SAED pattern (inset); f) dark-field image taken on the same area with e).

of the particles, which is in agreement with the nitrogen sorption results. In the HR-TEM images (Figure 2c and d), some bright regions are clearly observed through the whole particle, implying the presence of mesopores. Moreover, the apparently continuous and well-crystallized lattice fringes of the particle (Figure 2d) demonstrate the single-crystal nature of MZ. To investigate its hierarchical structure more thoroughly, the acquisition of projection images was also performed with scanning transmission electron microscopy (STEM), as shown in Figure 2e and f. The selected-area electron diffraction (SAED) pattern (Figure 2e, inset) verifies that the particle is a single crystal. It can be seen that some dark regions are dispersed over the bright contrast, as arrows point in Figure 2f, displaying as a bright contrast in the bright-field image inversely (Figure 2e). As this mode is mass-thickness sensitive, it can be concluded that mesoporous ZSM-5 was fabricated successfully, in which mesopores co-existed with three-dimensional microporosity of zeolite framework.

The structural configuration and the local environment of Si and Al atoms were investigated by ^{29}Si and ^{27}Al MAS NMR spectroscopy as shown in Figure 3. It is found that MZ and conventional

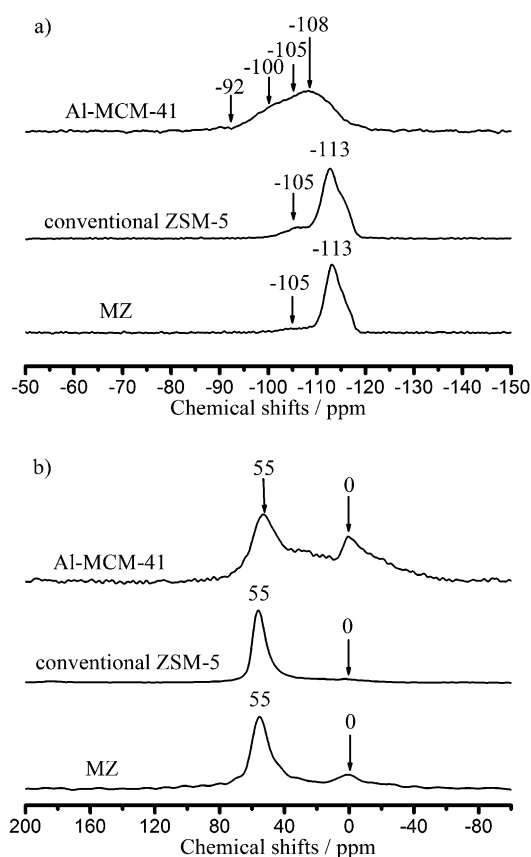


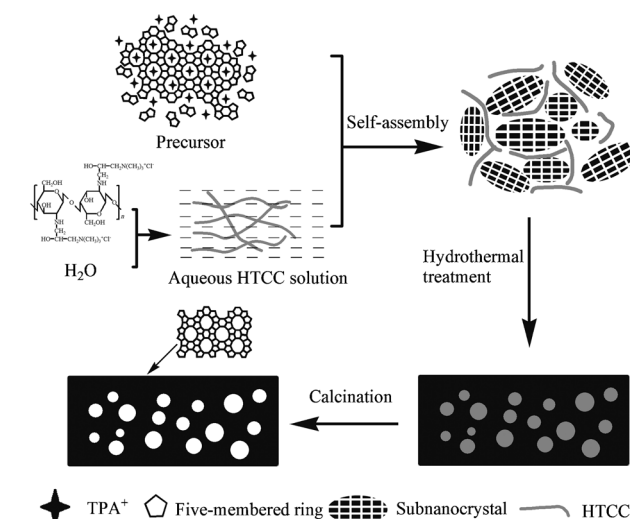
Figure 3. a) ^{29}Si and b) ^{27}Al MAS NMR spectra of MZ, conventional ZSM-5 and Al-MCM-41.

ZSM-5 display similar ^{29}Si MAS NMR spectra, both showing one major peak at $\delta = -113$ ppm and a weak shoulder at $\delta = -105$ ppm, which correspond to $\text{Si}(\text{OSi})_4$ (Q^4) and $(\text{AlO})_1\text{Si}(\text{OSi})_3$, respectively. On the contrary, three peaks and one shoulder with chemical shifts of $\delta = -92$, -100 , -108 , and -105 ppm are observed in Al-MCM-41, which can be ascribed to $(\text{HO})_2\text{Si}(\text{OSi})_2$ (Q^2), $(\text{HO})\text{Si}(\text{OSi})_3$ (Q^3), $\text{Si}(\text{OSi})_4$ (Q^4), and $(\text{AlO})_1\text{Si}(\text{OSi})_3$, respectively. The remarkably higher Q^4/Q^3 ratio of MZ indicates its higher condensation level compared with that of amorphous Al-MCM-41. The ^{27}Al MAS NMR spectra of both conventional ZSM-5 and MZ exhibit a pronounced peak centered at around $\delta = 55$ ppm and a weak peak centered at around $\delta = 0$ ppm that can be attributed to aluminum species with tetrahedral and octahedral coordination, respectively. This result demonstrates that most Al atoms in MZ have been incorporated into the framework dominantly as can be judged from its weak peak at $\delta = 0$ ppm. Correspondingly, it can be inferred that MZ and conventional ZSM-5 possess similar acidic properties with higher concentration of strong or medium acid sites than that of Al-MCM-41.

Thermogravimetric analyses (TGA) were performed to estimate the entrapment and amount of polymer HTCC during the synthesis of MZ. As shown in Figure S3a in the Supporting Information, HTCC shows three distinct steps in the weight loss. Reduction of the sample below 150°C can

be attributed to the release of adsorbed water. The weight losses of about 48.5 and 41.3% at $240\text{--}340^\circ\text{C}$ and $340\text{--}570^\circ\text{C}$ correspond to the different thermal degradation steps of HTCC.^[18] At 570°C or above, HTCC decomposed completely. Conventional ZSM-5 zeolite shows a weight loss of 11.8% attributable to the loss of water and the decomposition of TPAOH (Figure S3b in the Supporting Information). The as-synthesized MZ displays a weight loss of 17.5% at 800°C . The slight weight loss below 150°C is due to the removal of adsorbed water in MZ. The distinct weight loss of 1.9% within $240\text{--}350^\circ\text{C}$ can be ascribed to the initial decomposition of HTCC. However, the further decomposition of HTCC between 340 and 570°C overlaps with that of TPAOH, which is usually at $440\text{--}510^\circ\text{C}$.^[12e] Therefore, it can be estimated that the amount of polymer entrapped within crystals is about 3.5%. It is noteworthy that the higher weight loss in MZ than that in conventional ZSM-5 demonstrates that more organics were entrapped in the as-synthesized sample MZ, acting like a meso-template.

It is evident that the formation of MZ should be ascribed to the introduction of cationic polymer HTCC. Thus, we propose a Scheme for the synthesis of MZ under hydrothermal condition as shown in Scheme 1. Zeolite precursors



Scheme 1. Proposed route for the synthesis of MZ by the self-assembly between the zeolite precursor and HTCC under hydrothermal conditions.

were prepared according to the previous work.^[13k] After the addition of HTCC solution into the zeolite precursors, self-assembly between the zeolite precursors and cationic HTCC molecules took place through strong static interactions, forming the subnanocrystals/polymer composite. Then, hierarchical zeolite crystals with penetrating HTCC were synthesized during the hydrothermal treatment. Finally, mesoporous ZSM-5 particles were obtained after the removal of organic HTCC and TPAOH by calcination. It is noteworthy that the process proposed here is different from those proposed in the literature elsewhere, in which cationic polymer

served as a flocculating agent to form stable, easily retrievable aggregates.^[12f,19]

Figure 4 shows the temperature-programmed desorption of ammonia (NH₃-TPD) profiles of MZ, conventional ZSM-5 and Al-MCM-41 with the same Si/Al ratio of 50. Apparently, the profile of MZ is more alike to that of conventional ZSM-5, indicating their similar acidic features despite of

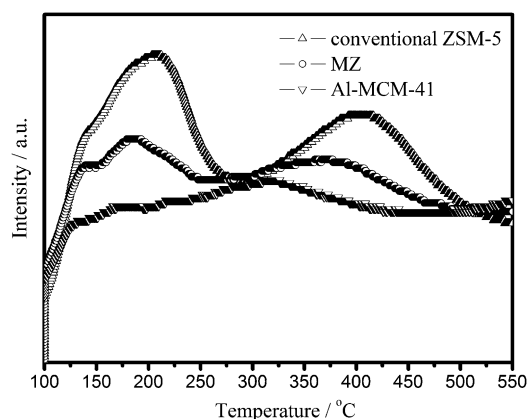
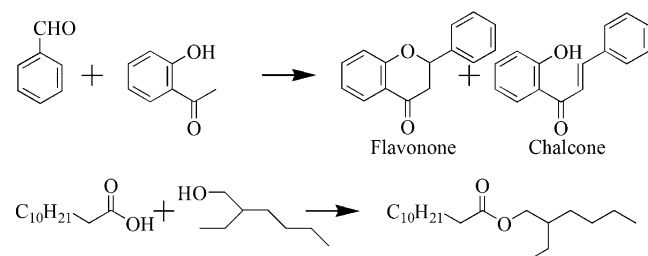


Figure 4. NH₃-TPD profiles of conventional ZSM-5, MZ and Al-MCM-41.

its relatively lower amount of NH₃ desorption. Moreover, it is observed that the NH₃ desorption temperature of sample MZ (380°C) is much higher than that of Al-MCM-41 (310°C) and the amount of NH₃ desorbed from MZ is significantly higher than that of Al-MCM-41, revealing the higher concentration/strength of acid sites in MZ.

Catalytic reactions involving large molecules, the Claisen–Schmidt condensation of 2-hydroxyacetophenone with benzaldehyde and the esterification reaction of lauric acid with 2-ethylhexanol (Scheme 2), were performed to verify the catalytic activity of MZ. Flavonoids have been found a wide range of applications, such as UV protection, flower coloration, interspecies interactions and plant defense, and they can also offer nutritional and medicinal values to humans.^[20] Batch esterification reactions catalyzed by solid acids provides an alternate route to the manufacture of the main components of biodiesel.^[21] Table 2 summarizes the catalytic data. As expected, MZ shows higher catalytic activities



Scheme 2. Claisen–Schmidt condensation of 2-hydroxyacetophenone with benzaldehyde (top); esterification reaction of lauric acid with 2-ethylhexanol (bottom).

Table 2. Catalytic properties of MZ and other aluminosilicate materials.^[a]

Reactions	MZ (Si/Al=50)	Conventional ZSM-5 (Si/Al=50)	Al-MCM-41 (Si/Al=50)
2-hydroxyacetophenone + benzaldehyde	22.8 (38:62:0) ^[b]	6.4 (40/60/0)	17.4 (67:33:0)
lauric acid + 2-ethylhexanol	14.0	8.1	10.7

[a] Catalytic properties were compared on the basis of the same weight of the catalysts (see the Experimental Section for details). All catalysts had the same Si/Al ratio of 50. [b] The first data value represents the reactant conversion [%]. The numbers in parentheses indicate the percentage selectivity of flavanone/chalcone/others.

(22.8, 14.0%) than either amorphous Al-MCM-41 (17.4, 10.7%) or bulky ZSM-5 (6.4, 8.1%) in both reactions. Compared with conventional ZSM-5, the higher activities of MZ should be ascribed to the introduction of intracrystalline mesopores, enhancing the efficient diffusion of reactant/product molecules through the solid catalyst. It was reported that the condensation reaction would occur at the external surface Al species irrespective of their acidic strength.^[22] Thus, the higher activity of MZ (22.8%) than that of Al-MCM-41 (17.4%) in the condensation reaction may be also caused by the creation of relatively larger mesopores of about 5–20 nm, which is much larger than that of Al-MCM-41 (2.7 nm), taking the higher Al_{external}/Al_{framework} ratio for Al-MCM-41 into account. It is well known that the esterification reaction of such bulky molecules requires a catalyst with strong acid sites. Thus, the better performance of MZ than Al-MCM-41 in the esterification reaction of lauric acid with 2-ethylhexanol perhaps can be attributed to the higher concentration of medium and strong acid sites in MZ, as shown in Figure 4.

Conclusion

A hierarchically porous aluminosilicate with micro/mesoporous structure, mesoporous ZSM-5, has been successfully synthesized by a conventional hydrothermal method using ammonium-modified chitosan and TPAOH as the meso- and microscale template, respectively. Various characterization technologies revealed that mesoporosity of about 5–20 nm in diameter coexisted with micropore network within uniform mesoporous ZSM-5 crystals. It was demonstrated that the ammonium-modified chitosan served as a mesopore, which can self-assemble with the zeolite precursor through strong static interactions, forming mesoporous zeolite ZSM-5. Due to the high specific surface area, external specific surface area, total pore volume, external volume and high concentration of medium and strong acid sites, mesoporous ZSM-5 exhibited significantly enhanced catalytic activities compared with conventional ZSM-5 and Al-MCM-41 in reactions involving bulky molecules. It is expected that this synthetic strategy can be applied to other structured zeolites, such as Y, TS-1, Beta zeolites, and so on.

Experimental Section

Synthesis of HTCC: The ammonium-modified chitosan, *N*-(2-hydroxy)propyl-3-trimethyl ammonium chitosan chloride (HTCC) was synthesized according to a method described elsewhere.^[17] Chitosan with a molecular weight of 100 000 gmol⁻¹ was used here.

Synthesis of mesoporous ZSM-5: In a typical synthesis, Al(*i*Pro)₃ (0.31 g, 1.50 mol) and TEOS (15.62 g, 0.075 mol) were mixed with deionized water (25.92 g), forming an oil-in-water emulsion at room temperature. After stirring for 2 h, TPAOH (25% aqueous, 21.96 g, 0.027 mol) was added into the resultant emulsion dropwise, which became a clear solution after stirring at 40 °C for 2–3 h. Then, the temperature was raised to 100 °C and maintained for 2 days. The molar ratio in the precursor was Al(*i*Pro)₃/TPAOH/TEOS/H₂O = 1:18:50:1570, and the entire reaction was carried out in a closed Schott Duran bottle.

After cooling the precursor solution to room temperature, the suspension was mixed with an aqueous solution of HTCC and stirred for 2 h at 80 °C. At last, the obtained earth yellow mixture was charged into Teflon-lined steel autoclaves for hydrothermal treatment at 150 °C for 18 h. The final products were filtered, washed with deionized water, dried overnight at 100 °C and calcined at 650 °C for 10 h. The obtained sample was designated as MZ. For comparison, conventional ZSM-5 and Al-MCM-41 with Si/Al = 50 were also synthesized according to the literature procedures.^[13e,23] All the samples were converted into the H-form by ion exchanges with 1 M NH₄NO₃ solution at 80 °C for three times and subsequent calcination in air at 550 °C for 5 h.

Characterization: Fourier transform infrared spectroscopy (FTIR) measurements were performed on a Nicolet 5700 FTIR spectrometer. Powder XRD patterns were collected on Bruker D8 Focus diffractometer with a graphite-monochromatized Cu_{Kα} radiation (λ = 0.15405 nm), typically run at a voltage of 40 kV and current of 40 mA. The N₂ adsorption isotherms were measured using Quantachrome NOVA 4200e. The specific surface area and pore size distribution were calculated by using the Brunauer–Emmett–Teller (BET) and Barrett–Joyner–Halenda (BJH) method, respectively. The micropore surface area and volume were calculated by the t-plot method; the total pore volume was evaluated at P/P₀ = 0.98. Field emission scanning electron microscopy (FE-SEM) images were obtained using a Hitachi S4800 electron microscope. Transmission electron microscopy (TEM) observations were performed on a JEOL-2010F electron microscope operated at 200 kV. The TG analysis was carried out under the atmosphere of air at a heating rate of 10 °C min⁻¹ using a NETZSCH STA 409 PG/PC instrument. ²⁹Si and ²⁷Al MAS NMR spectra were recorded on a Bruker AVANCE 600 spectrometer. Temperature-programmed desorption of ammonia (NH₃-TPD) was conducted on a homemade apparatus loaded with 200 mg of sample. The catalyst was pretreated at 550 °C for 1 h and then cooled down to 100 °C under He flow. Pure NH₃ was introduced until adsorption saturation was reached. The gaseous or physisorbed NH₃ was removed by purging He flow at 100 °C for 1 h. Then the temperature was raised from 100 to 550 °C with a heating rate of 1 °C min⁻¹ and the desorbed NH₃ was detected by gas chromatography. The ratios of Si/Al in different samples were determined by the results of inductively coupled plasma analysis (Thermo Elemental IRIS 1000).

Catalytic reactions: The Claisen–Schmidt condensation was carried out under N₂ atmosphere in a 25 mL three-necked flask equipped with a reflux condenser. A reaction mixture containing benzaldehyde (0.75 g, 7 mmol), 2-hydroxyacetophenone (0.476 g, 3.5 mmol) and catalyst (50 mg) was heated under stirring for 8 h at 150 °C. After the reaction, the mixture was cooled, centrifuged, diluted with acetone and analyzed by GC-MS (Agilent, 7890/5975C). The esterification was also performed in a 25 mL three-necked flask equipped with a reflux condenser. Typically, lauric acid (6.04 g, 0.03 mol), 2-ethylhexanol (3.99 g, 0.03 mol), freshly activated catalyst (0.1 g) and internal standard dodecane (100 μL, 0.44 mmol) were placed into the reactor and stirred for 2 h at 130 °C. After the reaction, the products were dissolved by adding a specific amount of acetone after centrifugation and analyzed by GC-MS (Agilent, 7890/5975C).

Acknowledgements

This work was financially supported by the National Basic Research Program of China (973 Program, 2012CB933602); Program for New Century Excellent Talents in University (NCET-10-0379); Scientific Innovation Project of Shanghai Municipal Education Commission (Grant No. 11ZZ53); The National Natural Science Foundation of China (Grant Nos. 51172070, 51132009), The Fundamental Research Funds for the Central Universities (Grant No. WD1114002 and WK1013001).

- [1] a) Y. Tao, H. Kanoh, L. Abrams, K. Kaneko, *Chem. Rev.* **2006**, *106*, 896–910; b) P. Adelhelm, Y. S. Hu, L. Chuenchom, M. Antonietti, B. M. Smarsly, J. Maier, *Adv. Mater.* **2007**, *19*, 4012–4017; c) Y. Deng, C. Liu, T. Yu, F. Liu, F. Zhang, Y. Wan, L. Zhang, C. Wang, B. Tu, P. A. Webley, H. Wang, D. Zhao, *Chem. Mater.* **2007**, *19*, 3271–3277; d) J. Pérez-Ramírez, C. H. Christensen, K. Egeblad, C. H. Christensen, J. C. Groen, *Chem. Soc. Rev.* **2008**, *37*, 2530–2542; e) D.-W. Wang, F. Li, M. Liu, G. Q. Lu, H.-M. Cheng, *Angew. Chem.* **2008**, *120*, 379–382; *Angew. Chem. Int. Ed.* **2008**, *47*, 373–376; f) Z. Wang, E. R. Kiesel, A. Stein, *J. Mater. Chem.* **2008**, *18*, 2194–2200; g) J. A. Martens, J. W. Thybaut, J. F. M. Denayer, S. P. Sree, A. Aerts, M.-F. Reyniers, V. VanSpeybroeck, M. Waroquier, A. Buekenhoudt, I. Vankelecom, W. Buijs, J. Persoons, G. V. Baron, S. Bals, G. Van Tendeloo, G. B. Marin, P. A. Jacobs, C. E. A. Kirschhock, *Catal. Today* **2011**, *168*, 17–27.
- [2] a) A. Corma, *Chem. Rev.* **1997**, *97*, 2373–2420; b) M. E. Davis, *Nature* **2002**, *417*, 813–821; c) C. S. Cundy, P. A. Cox, *Chem. Rev.* **2003**, *103*, 663–702.
- [3] a) B. J. Schoeman, J. Sterte, J. E. Otterstedt, *Zeolites* **1994**, *14*, 110–116; b) M. Hartmann, *Angew. Chem.* **2004**, *116*, 6004–6006; *Angew. Chem. Int. Ed.* **2004**, *43*, 5880–5882; c) J. Čejka, S. Mintova, *Catal. Rev. Sci. Eng.* **2007**, *49*, 457–509.
- [4] a) C. Madsen, C. J. H. Jacobsen, *Chem. Commun.* **1999**, 673–674; b) R. Srivastava, N. Iwasa, S.-i. Fujita, M. Arai, *Chem. Eur. J.* **2008**, *14*, 9507–9511.
- [5] J. Sun, C. Bonneau, A. Cantin, A. Corma, M. J. Diaz-Cabanas, M. Moliner, D. Zhang, M. Li, X. Zou, *Nature* **2009**, *458*, 1154–1157.
- [6] F. Ocampo, H. S. Yun, M. M. Pereira, J. P. Tessonnier, B. Louis, *Cryst. Growth Des.* **2009**, *9*, 3721–3729.
- [7] a) C. T. Kresge, M. E. Leonowicz, W. J. Roth, J. C. Vartuli, J. S. Beck, *Nature* **1992**, *359*, 710–712; b) P. T. Tanev, M. Chibwe, T. J. Pinnavaia, *Nature* **1994**, *368*, 321–323; c) D. Zhao, J. Feng, Q. Huo, N. Melosh, G. H. Fredrickson, B. F. Chmelka, G. D. Stucky, *Science* **1998**, *279*, 548–552.
- [8] X. Meng, F. Nawaz, F.-S. Xiao, *Nano Today* **2009**, *4*, 292–301.
- [9] a) A. H. Janssen, A. J. Koster, K. P. de Jong, *Angew. Chem.* **2001**, *113*, 1136–1138; *Angew. Chem. Int. Ed.* **2001**, *40*, 1102–1104; b) A. H. Janssen, A. J. Koster, K. P. de Jong, *J. Phys. Chem. B* **2002**, *106*, 11905–11909; c) S. van Donk, A. H. Janssen, J. H. Bitter, K. P. de Jong, *Catal. Rev. Sci. Eng.* **2003**, *45*, 297–319; d) J. C. Groen, L. A. A. Peffer, J. A. Moulijn, J. Pérez-Ramírez, *Chem. Eur. J.* **2005**, *11*, 4983–4994; e) C. Mei, Z. Liu, P. Wen, Z. Xie, W. Hua, Z. Gao, *J. Mater. Chem.* **2008**, *18*, 3496–3500; f) J. Pérez-Ramírez, S. Abelló, L. A. Villaescusa, A. Bonilla, *Angew. Chem.* **2008**, *120*, 8031–8035; *Angew. Chem. Int. Ed.* **2008**, *47*, 7913–7917.
- [10] a) W. Han, Y. Jia, N. Yao, W. Yang, M. He, G. Xiong, *J. Sol-Gel Sci. Technol.* **2007**, *43*, 205–211; b) L. Chen, S. Y. Zhu, Y. M. Wang, M.-Y. He, *New J. Chem.* **2010**, *34*, 2328–2334.
- [11] a) C. J. H. Jacobsen, C. Madsen, J. Houzvicka, I. Schmidt, A. Carlsson, *J. Am. Chem. Soc.* **2000**, *122*, 7116–7117; b) I. Schmidt, A. Boisen, E. Gustavsson, K. Ståhl, S. Pehrson, S. Dahl, A. Carlsson, C. J. H. Jacobsen, *Chem. Mater.* **2001**, *13*, 4416–4418; c) Y. Tao, H. Kanoh, K. Kaneko, *J. Am. Chem. Soc.* **2003**, *125*, 6044–6045; d) A. Sakthivel, S.-J. Huang, W.-H. Chen, Z.-H. Lan, K.-H. Chen, T.-W. Kim, R. Ryoo, A. S. T. Chiang, S.-B. Liu, *Chem. Mater.* **2004**, *16*, 3168–3175; e) K. Egeblad, M. Kustova, S. K. Klitgaard, K. Zhu, C. H. Christensen, *Microporous Mesoporous Mater.* **2007**, *101*, 214–223; f) W. Fan, M. A. Snyder, S. Kumar, P.-S. Lee, W. C. Yoo, A. V.

- McCormick, R. Lee Penn, A. Stein, M. Tsapatsis, *Nat. Mater.* **2008**, *7*, 984–991.
- [12] a) Y. Tao, H. Kanoh, K. Kaneko, *Langmuir* **2005**, *21*, 504–507; b) H. Wang, T. J. Pinnavaia, *Angew. Chem.* **2006**, *118*, 7765–7768; *Angew. Chem. Int. Ed.* **2006**, *45*, 7603–7606; c) F.-S. Xiao, L. Wang, C. Yin, K. Lin, Y. Di, J. Li, R. Xu, D. S. Su, R. Schlögl, T. Yokoi, T. Tatsumi, *Angew. Chem.* **2006**, *118*, 3162–3165; *Angew. Chem. Int. Ed.* **2006**, *45*, 3090–3093; d) H. Zhu, Z. Liu, D. Kong, Y. Wang, Z. Xie, *J. Phys. Chem. C* **2008**, *112*, 17257–17264; e) L. Wang, Z. Zhang, C. Yin, Z. Shan, F.-S. Xiao, *Microporous Mesoporous Mater.* **2010**, *131*, 58–67; f) K. Möller, B. Yilmaz, U. Müller, T. Bein, *Chem. Mater.* **2011**, *23*, 4301–4310; g) J. Zhou, Z. Hua, Z. Liu, W. Wu, Y. Zhu, J. Shi, *ACS Catal.* **2011**, *1*, 287–291.
- [13] a) Y. Liu, W. Zhang, T. J. Pinnavaia, *J. Am. Chem. Soc.* **2000**, *122*, 8791–8792; b) S. P. B. Kremer, C. E. A. Kirschhock, A. Aerts, K. Villani, J. A. Martens, O. I. Lebedev, G. Van Tendeloo, *Adv. Mater.* **2003**, *15*, 1705–1707; c) C. E. A. Kirschhock, S. P. B. Kremer, J. Vermant, G. Van Tendeloo, P. A. Jacobs, J. A. Martens, *Chem. Eur. J.* **2005**, *11*, 4306–4313; d) S. P. B. Kremer, C. E. A. Kirschhock, A. Aerts, C. A. Aerts, K. J. Houthoofd, P. J. Grobet, P. A. Jacobs, O. I. Lebedev, G. Van Tendeloo, J. A. Martens, *Solid State Sci.* **2005**, *7*, 861–867; e) M. Choi, H. S. Cho, R. Srivastava, C. Venkatesan, D.-H. Choi, R. Ryoo, *Nat. Mater.* **2006**, *5*, 718–723; f) S. Bals, K. J. Batenburg, D. Liang, O. Lebedev, G. Van Tendeloo, A. Aerts, J. A. Martens, C. E. A. Kirschhock, *J. Am. Chem. Soc.* **2009**, *131*, 4769–4773; g) M. Choi, K. Na, J. Kim, Y. Sakamoto, O. Terasaki, R. Ryoo, *Nature* **2009**, *461*, 246–249; h) J. Zhao, Z. Hua, Z. Liu, Y. Li, L. Guo, W. Bu, X. Cui, M. Ruan, H. Chen, J. Shi, *Chem. Commun.* **2009**, 7578–7580; i) H. Li, J. Jin, W. Wu, C. Chen, L. Li, Y. Li, W. Zhao, J. Gu, G. Chen, J.-l. Shi, *J. Mater. Chem.* **2011**, *21*, 19395–19401; j) K. Na, C. Jo, J. Kim, K. Cho, J. Jung, Y. Seo, R. J. Messinger, B. F. Chmelka, R. Ryoo, *Science* **2011**, *333*, 328–332; k) Y. Zhu, Z. Hua, J. Zhou, L. Wang, J. Zhao, Y. Gong, W. Wu, M. Ruan, J. Shi, *Chem. Eur. J.* **2011**, *17*, 14618–14627.
- [14] H. Zhu, Z. Liu, Y. Wang, D. Kong, X. Yuan, Z. Xie, *Chem. Mater.* **2008**, *20*, 1134–1139.
- [15] a) J. Retuert, R. Quijada, V. Arias, *Chem. Mater.* **1998**, *10*, 3923–3927; b) J. Retuert, R. Quijada, V. Arias, M. Yazdani-Pedram, *J. Mater. Res.* **2003**, *18*, 487–494; c) H. V. Fajardo, A. O. Martins, R. M. deAlmeida, L. K. Noda, L. F. D. Probst, N. L. V. Carreño, A. Valentini, *Mater. Lett.* **2005**, *59*, 3963–3967.
- [16] M. Falco, J. Retuert, A. Hidrobo, C. Covarrubias, P. Araya, U. Sedran, *Appl. Catal. A* **2009**, *366*, 269–274.
- [17] C.-W. Nam, Y.-H. Kim, S.-W. Ko, *J. Appl. Polym. Sci.* **1999**, *74*, 2258–2265.
- [18] L. Zeng, C. Qin, L. Wang, W. Li, *Carbohydr. Polym.* **2011**, *83*, 1553–1557.
- [19] J. Song, L. Ren, C. Yin, Y. Ji, Z. Wu, J. Li, F.-S. Xiao, *J. Phys. Chem. C* **2008**, *112*, 8609–8613.
- [20] S. Martens, A. Mithöfer, *Phytochemistry* **2005**, *66*, 2399–2407.
- [21] A. A. Kiss, A. C. Dimian, G. Rothenberg, *Adv. Synth. Catal.* **2006**, *348*, 75–81.
- [22] V. N. Shetti, J. Kim, R. Srivastava, M. Choi, R. Ryoo, *J. Catal.* **2008**, *254*, 296–303.
- [23] R. Ryoo, M. Jeong Kim, *Chem. Commun.* **1997**, 2225–2226.

Received: May 8, 2012

Revised: September 19, 2012

Published online: November 5, 2012